

Supplementary Materials for

Earth's water may have been inherited from material similar to enstatite chondrite meteorites

Laurette Piani, Yves Marrocchi, Thomas Rigaudier, Lionel G. Vacher, Dorian Thomassin, Bernard Marty

Correspondence to: laurette.piani@univ-lorraine.fr

This PDF file includes:

Materials and Methods

Supplementary Text

Figs. S1 to S6

Tables S1 to S6

Other Supplementary Materials for this manuscript:

Data S1

Materials and Methods

Samples

Bulk-rock hydrogen concentrations and isotopic compositions were measured in thirteen enstatite chondrites and one aubrite, and in three carbonaceous chondrites for reference (Table S2). Meteorite samples were provided by the Field Museum (Chicago, USA) for Indarch, St Mark's, Daniel's Kuil, Eagle, Hvittis, Khaipur and Pillistfer, the French National Museum of Natural History (Paris, France) for Saint Sauveur, Abee, Kota-Kota, Orgueil, Alais and Muchison, the Japanese National Institute for Polar Research (Tokyo, Japan) for Yamato-791790, the University of New Mexico (Albuquerque, USA) for Norton County, and CEREGE meteorite collection (France) for Caleta el Cobre 025. Remaining pieces of the samples are currently archived at CRPG for further analyses of volatile elements; surviving pieces, if any, will be returned to the collections after completion. A resin-free polished section of Sahara 97096 (12) was provided by the French National Museum of Natural History for SIMS measurements of the hydrogen contents and isotopic compositions in chondrule mesostasis. The sample was gold coated and inserted in the instrument several days before analyses. Although the outer part of the Sahara 97096 and of its paired fragments, such as Sahara 97116, were exposed to terrestrial weathering, the inner parts, from which our samples were taken, remained fresh and did not experience terrestrial fluid circulation, as attested by presence of pristine oldhamite, a highly hydrophilic calcium-rich sulfide (14, 15) (Fig. S1). Compared to Sahara 97096, the total mass of Caleta el Cobre 025 is much less (< 800g comparing with 28 kg) and the sample might thus have been more pervasively altered. Even the most pristine pieces of Caleta el Cobre 025 we obtained show slight oxidation rims around oldhamite that may contribute to the H budget measured in bulk rock. The Kota-Kota EH3 chondrite is a 334-gram-stone that was found in 1905 in Malawi. The Kota-Kota chondrite also contains pervasive marks of terrestrial alteration (36). The bulk rock results for these two meteorites are reported below but not included in the discussion, due to their possible terrestrial contamination. Chondrule mesostases from the two CV-type carbonaceous chondrites Kaba (CV3oxB, provided by the Natural History Museum of Vienna, Austria) and Vigarano (CV3red, provided by the French National Museum of Natural History) were also analyzed by SIMS for comparison.

Bulk-rock analyses

Fresh pieces of the enstatite chondrites (50–100 mg) were crushed, homogenized, and divided into aliquots of 10–16 mg for measurement of bulk-rock hydrogen abundances and isotopic compositions. Additionally, 16-mg aliquots were also taken from powders previously prepared from three different lithologies of the brecciated aubrite Norton County: a dark lithology, a grey lithology, and from isolated large enstatite crystals (37). Hydrogen abundances and isotopic compositions were analyzed using a Thermo Scientific EA IsoLink-deltaV IRMS System at the CRPG laboratory (Nancy, France) following published procedures (38). The samples were weighed, wrapped in tin capsules, and degassed at 120 °C under vacuum for 48 h in a degassing canister to remove adsorbed water (38). After dehydration, the degassing canister was placed in a dry, N₂-flushed glovebox and the tin capsules were transferred to a custom sealed, auto-sampler pre-flushed with He. This step avoids exposure of the samples to atmospheric moisture, which could rapidly re-hydrate them, and increases the reproducibility of H content and D/H measurements (38). The sealed auto-sampler was then connected to the EA and evacuated for at least 20 min before opening to the reduction column. Pyrolysis of the samples was performed at

1450 °C on an EA glassy carbon reaction tube packed with glassy carbon chips and enclosed in a ceramic liner to reduce hydroxyls to H₂. After chromatographic separation, the evolved H₂ was introduced into the mass spectrometer and its D/H isotopic composition analyzed. The amount of H₂ produced was estimated by comparison of the thermal conductivity detector peak area with the signal produced during the analysis of internal standards: two micas, Mica-Mg and Musc D65, and a marine sediment SO 188 (38). In addition to water-rich internal standards (2.58, 4.34, and 4.36 wt.% H₂O, respectively), four mid-ocean ridge basalts (MORBs) were also used to estimate the reproducibility of the hydrogen concentration measured for samples with moderate hydrogen-contents (CYP78, GSJ-JB3, SR2-02, and GMR-KS12 containing 0.14, 0.20, 0.27, and 0.42 wt.% H₂O, respectively). CYP78, SR2-02, and GMR-KS12 are CRPG internal standards and GSJ-JB3 is from the Geological Survey of Japan (39). The detection limit of the EA-IRMS measurements was estimated to ~0.05 wt.% H₂O using empty tin capsules. The reproducibility on hydrogen concentrations, calculated as two times the standard deviation divided by the average (Table S1), increases with decreasing water content following a negative power law (Fig. S2). This negative power law ($2SD/[H] = 0.05 \times [H]^{-0.43}$, where SD is the standard deviation and [H] is the hydrogen concentration) was used to estimate the 2SD reproducibility of the samples, which is reported in Table S2. The uncertainty on the fit at 95% confidence is $\leq 10\%$ within the range of the meteorite sample hydrogen contents (Fig. S2). The three internal standards (Mica-Mg, Musc D65, and SO188) were routinely included during sample analyses to account for instrumental drift. These internal standards were calibrated against reference materials from the International Atomic Energy Agency (IAEA), NBS30 (biotite, $\delta D = 65.7\%$), NBS22 (oil, $\delta D = 120\%$), and CH-7 (polyethylene, $\delta D = 100.3\%$) (40), for D/H isotopic analyses and to monitor mass spectrometer linearity. Given the measured reproducibility of the hydrogen isotopic compositions of the standards, and replicate analyses on meteorites (e.g., Sahara 97116, four measurements, $2SD = 1.4\%$), we conservatively estimate an uncertainty of 5‰ on the δD values of the samples and plot this as error bars in our figures.

SIMS analyses

Hydrogen abundances in chondrule mesostases were measured with a CAMECA 1280 HR2 SIMS at the CRPG. A liquid nitrogen cold trap was used to reduce the H₂O background and maintain a pressure below 2×10^{-9} Torr in the analytical chamber. We used a 10-keV O⁻ primary ion beam produced in a Hyperion radio-frequency plasma source that produces a dense and stable primary ion current with higher secondary ion transmission than a Duoplasmatron O⁻ source and a Cs⁺ source (41). The negative primary ions obviate the use of an electron gun (and thus charge compensation), reducing both instability of the secondary signal and surficial hydrogen desorption by electrons that could perturb the measurements. Prior to analysis, 120 s of presputtering with a 10-nA current was applied over an area $10 \mu\text{m} \times 10 \mu\text{m}$ to remove the gold coating and reach the sputtering steady state. The samples were then measured with a 10-nA current rastered over the $10 \mu\text{m} \times 10 \mu\text{m}$ area. A small field aperture (1,800 μm) and 90% electronic gate were used to eliminate hydrogen contamination from the crater edges. The ¹H⁺, D⁺, ¹²C⁺, and ³⁰Si⁺ ions were collected sequentially by changing the magnetic field and counted with a monocollector electron multiplier. ¹H⁺ was measured twice successively: first with a 70-keV energy offset that was also applied on ³⁰Si⁺ to measure the ¹H⁺/³⁰Si⁺ ratio, then without an energy offset to measure the D⁺/H⁺ ratio. The use of the offset allows ³⁰Si⁺ to be measured on the electron multiplier even for the most SiO₂-rich samples and reduces the proportion of surficial hydrogen characterized by a lower energy. The mass resolution (M/ Δ M) was set to 4,000 to

avoid interferences of H_2^+ on $^2\text{H}^+$ and $^{29}\text{SiH}^+$ on $^{30}\text{Si}^+$ and obtain flat-topped peaks. H_2O concentrations and D/H compositions of chondrule mesostases were determined using seven glass standards including four basaltic (46.8–50.4 wt.% SiO_2), two andesitic (58.5–60.2 wt.% SiO_2), one dacitic (63.7 wt.% SiO_2), and one rhyolitic glass (76.4 wt.% SiO_2 , Table S3). All glasses except the rhyolite present a strong correlation between the secondary ion intensity ratios $^1\text{H}^+/^30\text{Si}^+$ and the known $\text{H}_2\text{O}/\text{SiO}_2$ abundances of the glass standards with no visible dependency on the SiO_2 content (correlation coefficient $r^2 = 0.997$, Fig. S3), consistent with previous studies at similar H_2O contents, e.g. (42). The measured $^1\text{H}^+/^30\text{Si}^+$ was slightly enhanced compared to the other standards. The basalt-andesite-dacite correlation was used to estimate the H_2O abundance of the Kaba and Vigarano chondrule mesostases, which have basaltic SiO_2 contents from 44.4 to 51.4 wt.%. The detection limit of water was estimated using San Carlos olivine [≤ 1 ppm H_2O (43)], for which we found a water content of 28 ± 2 ppm after correction for instrumental fractionation using the basalt-andesite-dacite correlation. For chondrule mesostases of the EH3 Sahara 97096 (54.8–69.2 wt.% SiO_2 ; Data S1), to avoid overestimating hydrogen abundances due to a possible instrumental effect on SiO_2 -rich glass, we corrected $^1\text{H}^+/^30\text{Si}^+$ for instrumental fractionation using both the basalt-andesite-dacite correlation and the rhyolite reference by applying a weighting coefficient as a function of SiO_2 content. Moreover, we used phonolitic glasses [10.7 wt.% Na_2O and 8.2 wt.% K_2O (44)] to confirm that our SIMS H_2O measurements were not dependent on alkaline-rich compositions in the range of $^1\text{H}^+/^30\text{Si}^+$ ratios measured for the chondrule mesostases (Fig. S3, Table S2). D/H ratios were corrected for instrumental mass fractionation using the average of the instrumental fractionation factors (α) calculated on all glass standards ($\alpha = (\text{D}^+/\text{H}^+)/(\text{D}/\text{H}_{\text{ref}}) = 0.74 \pm 0.02$, 2SE where SE = standard error of the mean, Table S3). The reproducibility on the D/H ratio in the homogeneous glass standards was $\sim 40\%$ (2σ).

Mixing of carbonaceous chondrite- and enstatite chondrite-type materials

We compute the proportion of enstatite and CI carbonaceous chondrites [CIs chosen to account for the neon isotopic composition of the atmosphere (5)] necessary to reproduce the H and N isotopic compositions of Earth's surface reservoirs (oceans + atmosphere) i.e. $\delta\text{D} \equiv 0\%$ and $\delta^{15}\text{N} \equiv 0\%$. The mixing equations are:

$$(m_{\text{H}_{\text{EC}}} + m_{\text{H}_{\text{CI}}}) \cdot \frac{\text{D}}{\text{H}_{\text{surf}}} = m_{\text{H}_{\text{EC}}} \cdot \frac{\text{D}}{\text{H}_{\text{EC}}} + m_{\text{H}_{\text{CI}}} \cdot \frac{\text{D}}{\text{H}_{\text{CI}}} \quad (\text{S1})$$

$$(m_{\text{N}_{\text{EC}}} + m_{\text{N}_{\text{CI}}}) \cdot \frac{^{15}\text{N}}{^{14}\text{N}_{\text{surf}}} = m_{\text{N}_{\text{EC}}} \cdot \frac{^{15}\text{N}}{^{14}\text{N}_{\text{EC}}} + m_{\text{N}_{\text{CI}}} \cdot \frac{^{15}\text{N}}{^{14}\text{N}_{\text{CI}}} \quad (\text{S2})$$

where the subscripts 'surf', 'CI', and 'EC' indicate Earth's surface reservoirs, CI chondrites, and enstatite chondrites, respectively, and m_{H} and m_{N} are the masses of H (water) and N, respectively, contributed to Earth's oceans and atmosphere by ECs and CIs.

If we define $\eta_{\text{CI}} = \frac{m_{\text{H}_{\text{CI}}}}{m_{\text{H}_{\text{EC}}} + m_{\text{H}_{\text{CI}}}}$ and $\lambda_{\text{CI}} = \frac{m_{\text{N}_{\text{CI}}}}{m_{\text{N}_{\text{EC}}} + m_{\text{N}_{\text{CI}}}}$, the fractions of surficial hydrogen and nitrogen inherited from CIs, we obtain:

$$\eta_{\text{CI}} = \frac{\text{D}/\text{H}_{\text{surf}} - \text{D}/\text{H}_{\text{EC}}}{\text{D}/\text{H}_{\text{CI}} - \text{D}/\text{H}_{\text{EC}}} \quad (\text{S3})$$

$$\lambda_{CI} = \frac{{}^{15}\text{N}/{}^{14}\text{N}_{\text{surf}} - {}^{15}\text{N}/{}^{14}\text{N}_{\text{EC}}}{{}^{15}\text{N}/{}^{14}\text{N}_{\text{CI}} - {}^{15}\text{N}/{}^{14}\text{N}_{\text{EC}}} \quad (\text{S4})$$

The relative masses of CI- and EC-type materials necessary to reproduce the H and N isotopic compositions of Earth's surface reservoirs (oceans + atmosphere) can be defined as:

$$\gamma_{CI} = \frac{m_{H_{CI}}}{[H_{CI}]} \quad \text{and} \quad \gamma_{EC} = \frac{m_{H_{EC}}}{[H_{EC}]} \quad \text{with} \quad \gamma_{CI} + \gamma_{EC} = 1$$

$$\varepsilon_{CI} = \frac{m_{N_{CI}}}{[N_{CI}]} \quad \text{and} \quad \varepsilon_{EC} = \frac{m_{N_{EC}}}{[N_{EC}]} \quad \text{with} \quad \varepsilon_{CI} + \varepsilon_{EC} = 1$$

where $[H_{CI}]$ and $[N_{CI}]$ are the concentrations of H and N in CI-type materials, respectively, and $[H_{EC}]$ and $[N_{EC}]$ are the concentrations of H and N in EC-type materials, respectively.

Using this formalism:

$$\eta_{CI} = \frac{m_{H_{CI}}}{m_{H_{EC}} + m_{H_{CI}}} = \frac{[H_{CI}] \cdot \gamma_{CI}}{[H_{EC}] \cdot (1 - \gamma_{CI}) + [H_{CI}] \cdot \gamma_{CI}} \quad (5)$$

γ_{CI} and ε_{CI} can then be computed as:

$$\gamma_{CI} = \frac{[H_{EC}] \cdot \eta_{CI}}{[H_{CI}] + \eta_{CI} \cdot ([H_{EC}] - [H_{CI}])} \quad (6)$$

and

$$\varepsilon_{CI} = \frac{[N_{EC}] \cdot \lambda_{CI}}{[N_{CI}] + \lambda_{CI} \cdot ([N_{EC}] - [N_{CI}])} \quad (7)$$

and estimated from the H and N abundances and isotopic compositions of EC- and CI-type chondrites and from the H and N isotopic compositions of Earth's surface.

Taken the values summarized in Table S5, we obtain $\gamma_{CI} = 4\%$, indicating that the H isotopic composition of Earth's surface reservoir requires a mixture of 4% CI-type material and 96% EC-type material. From N contents and isotopic compositions, we obtain $\varepsilon_{CI} = 15\%$, higher than in the case of H, and indicating a possible cometary contribution to the N isotopic composition of Earth's surface (see below).

Supplementary Text

Cometary contribution

A cometary contribution to the atmosphere and oceans could have also shifted their H and N isotopic signatures. Xe isotopes measured in comet 67P/Churyumov-Gerasimenko, suggest that 10^{21} – 10^{22} g of cometary material could have impacted the Earth (45). Such a late delivery of volatiles could have contributed 0.5–5% N of Earth's atmospheric N [based on the cometary

composition (29)]. Considering cometary $\delta^{15}\text{N}$ values of roughly +1,000‰ (46), Earth's surface inventory would have been enriched in ^{15}N by 5–50‰, in the range of the observed N isotopic difference between the mantle and the atmosphere. For water [considering a cometary δD value of +3,000‰ (46)], the isotopic shift would have been smaller, in the range of 1–10‰ due to the smaller cometary contribution of H to Earth's water compared to nitrogen (29). Hence, contributions from 67P-like comets would have had a negligible impact on the H isotopic composition of Earth's oceans, but could have raised the N isotopic compositions of Earth's surface reservoirs.

EC hydrogen data in the literature

Few data have previously been reported for the hydrogen contents and, to a lesser extent, isotopic composition of bulk-rock enstatite chondrites (Table S6). Previously reported measurements were restricted to a small number of ECs (only one EH4 and one EL6 for hydrogen isotopes), with unknown terrestrial contamination on bulk-rock measurements. Published data show large variations (from <0.01 to 4.6 wt.% H_2O and δD from –135 to –68‰). No such high water contents or δD values were present in our data (Tables S2) for which the influence of terrestrial contamination was limited by the sample selection, preparation and analytical methodology.

Interpretation of Model #2

The water content brought by different proportions of enstatite, ordinary and carbonaceous chondrite-like materials (Fig. 2) are based on three end-member compositions for the composition of the Earth's building blocks, each taken from literature. Although Model #1 and 3 produce consistent isotopic compositions for the Earth's mantle (3), this might not be the case for Model #2, which includes 68% EC-like and 32% carbonaceous chondrite-like materials (2, 23). The calculated Earth's mantle composition using Model #2 for isotopic systems such as Cr, Ni, or Ti are inconsistent with terrestrial values, given the large deviations of CI-like materials with terrestrial values for these elements (3). Because the oxygen isotopic values of EC and CI are on, or very close to, the terrestrial fractionation line (i.e., $\delta^{17}\text{O} - 0.52 \times \delta^{18}\text{O} \approx 0$), a mixing of 32% of CIs to 68% of ECs would not affect the oxygen isotopic composition of the Earth characterized by $\Delta^{17}\text{O} = 0$. We consider our calculations to be extreme cases, to test if EC-like materials could account for the H content and isotopic composition of the Earth.

H content and isotope composition of the aubrite Norton County

The H content and isotope composition of the aubrite Norton County are in the range of those measured in metamorphosed chondrites. This similarity may be due to either: possible terrestrial contamination, as Norton County aliquots were taken from powders prepared for a previous study (37); or the speciation of hydrogen in reduced conditions which was partially preserved during melting on the aubrite parent body. Under reducing conditions, hydrogen combines with many elements such as carbon, nitrogen or sulfur to form C-H, N-H or S-H complexes in silicate melts (e.g., 47) and could also be dissolved as H_2 (e.g., 48). The volatile character of elements can change dramatically under reducing conditions: for example, sulfur, which is highly volatile under oxidizing conditions and can easily degas, becomes lithophile and remains concentrated in silicate melts under reducing conditions (49).

The high H content and the D/H ratio similar to ECs measured in Norton County are consistent with a limited loss of H during melting and a possible H-enrichment in the silicate fraction, compared to the metal fraction (50).

Effect of shocks on the degree of alteration in ECs

To estimate if shocks on parent bodies might have played a role in facilitating the terrestrial alteration and contamination of ECs, we investigated the relation between shock degrees, find and fall nature, D/H ratio and H content of the measured ECs (Fig. S5.A). Chondrites with the highest shock stage S3 (51) are at the lower end of the 1/H variation, so may contain more terrestrial contaminant than chondrites with a lower shock stage (S2). Similar water content and D/H ratios are obtained for both falls and finds, so terrestrial contamination is unlikely to explain the data.

Timing of the accretion of CI-like material

Given hydrogen, nitrogen and noble gas elemental and isotope data, we conclude that: i) the composition of surficial Earth volatile elements can be explained by adding a few percent of CI-like material to a predominantly EC-like material and ii) this add-mixing must have occurred sufficiently late to avoid large-scale degassing and global mantle re-homogenization. A remnant of solar-like neon seems to be preserved in the deep mantle sampled by mantle plumes (52, 53). The exact timing of accretion of CI-like material is then difficult to determine from our data. Oceans might have been present before the Moon forming impact (e.g. 54). Given the presence of 'EC-like' siderophile elements such as ruthenium or nickel (3, 55) in the mantle, the addition of the volatile-rich CI-like chondrites seems to have occurred during the main stages of terrestrial accretion and not as a 'late veneer'. CI-like material might have been scattered into the inner Solar System within a few Myr after calcium- aluminum-rich inclusion (CAI; the oldest dated solids in the Solar System) formation (10, 56), whereas late accretion occurred around, or after, the Moon forming event, a few tens of Myr later.

Enstatite chondrites are the earliest chondrites to accrete (around 2 Ma after CAIs), indicating that the EC reservoir was present when the primary accretion of the Earth began (at the earliest around 2.5 Ma after CAI) (57). Carbonaceous chondrites accreted a few million years later (3-4 Ma after CAI) but could still have contributed to the main stages of the Earth accretion, because 63% of the present-day Earth mass is thought to accrete within 11-24 Ma after CAI formation (58).

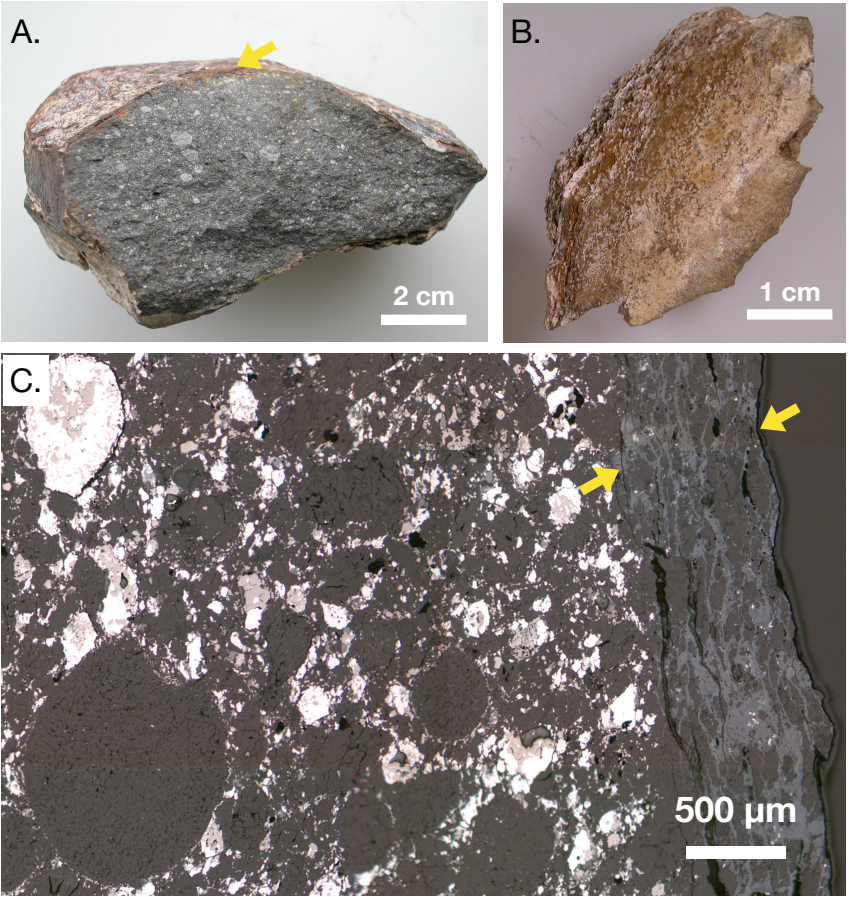


Fig. S1. Illustrations of the non-pervasive terrestrial alteration in the primitive enstatite chondrite Sahara 97096. A. Photograph of the fresh interior part of the enstatite chondrite Sahara 97096 (MNHN, Paris), showing a thin rusted border (yellow arrow) and a pristine interior. B. Photograph of the rusty exterior of the enstatite chondrite Sahara 97096 (12). C. Reflected light optical microscope image of a thick section of Sahara 97096 showing the sharp boundary between the weathered border (yellow arrows) and the pristine interior, which contains oldhamite, a highly hydrophilic calcium-rich sulfide (12, 14).

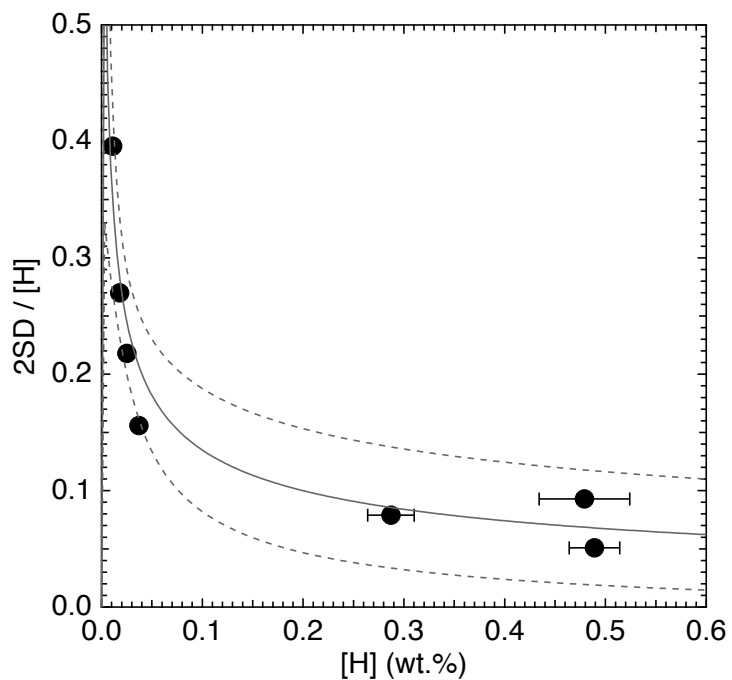


Fig. S2. Evolution of the relative reproducibility of the EA-IRMS measurement as a function of the hydrogen content. The black circles show the values obtained for the standards used for bulk H content measurements (Table S1), the grey line is the fit of the data obtained using a negative power law and the dotted lines represent the 95% confidence interval.

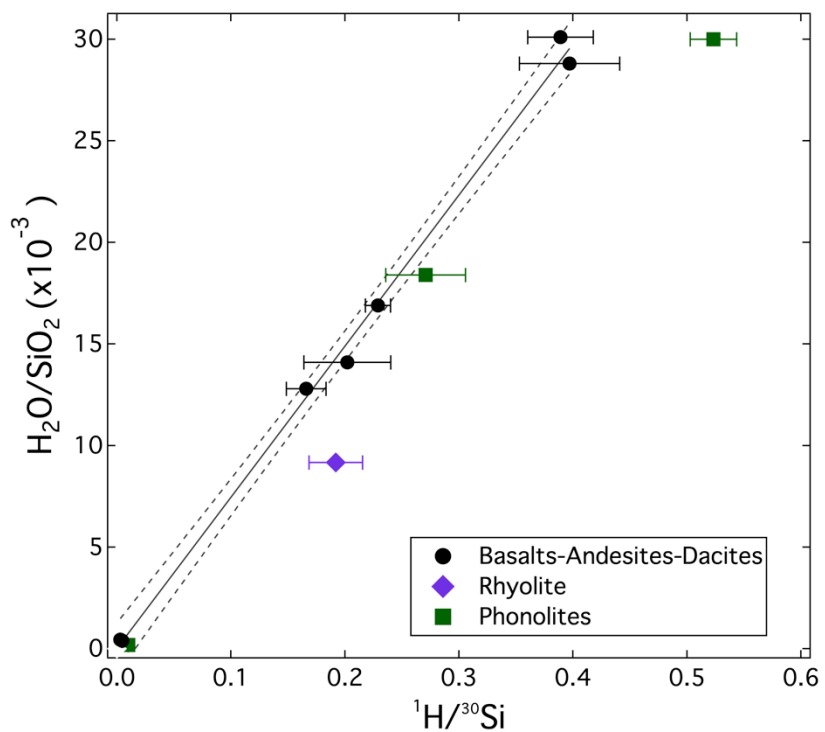


Fig. S3. Calibration of H content using SIMS. $^1\text{H}^{+}/^{30}\text{Si}^{+}$ vs. $\text{H}_2\text{O}/\text{SiO}_2$ relationship for the basalt-andesite-dacite glass standards (black circles, $r^2 = 0.997$), and comparison to the rhyolitic glass (purple diamond) and three phonolitic glass standards (green squares). The solid line corresponds to the linear fit of the basalt-andesite-dacite standards and dotted lines represent the 95% confidence interval.

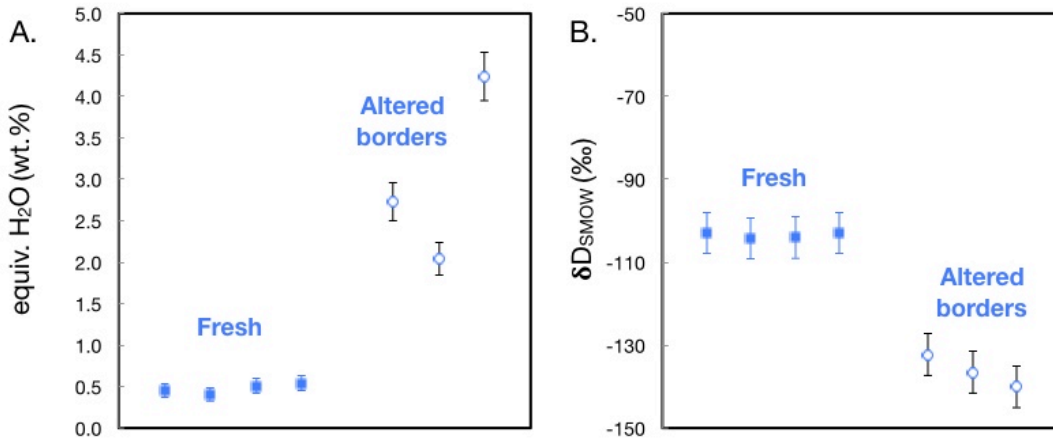


Fig. S4. Bulk (A) hydrogen contents and (B) isotopic compositions of fresh (plain squares) and terrestrially altered (open squares) pieces of the enstatite chondrite Sahara 97096. Hydrogen isotopic compositions are normalized against standard mean ocean water (SMOW, $D/H_{SMOW} = 0.00015576$). Error bars represent the 2σ uncertainties. Data are listed in Table S2.

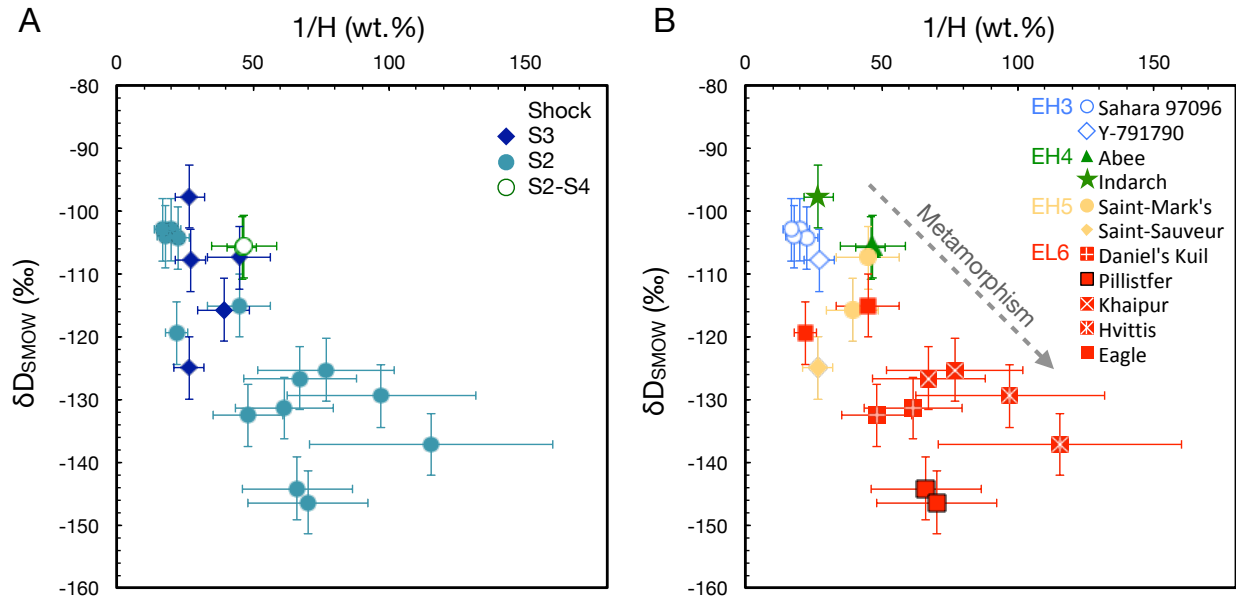


Fig. S5. Shock and metamorphism effects on the H content (expressed as 1/H) and isotopic distribution of ECs. (A) Distribution of the H content and isotopic composition measured in bulk enstatite chondrites indicating their shock stages (51). No clear trend is observed. The Abee chondrite, which is an impact melt breccia with a complex shock stage, has been reported as an open symbol. (B) Distribution of the H content and isotopic composition measured in bulk enstatite chondrites indicating their metamorphic degrees. Hydrogen contents and isotopic compositions decrease progressively with increasing degree of metamorphism (grey dashed arrow). Meteorite falls are reported as plain symbols; finds as open symbols. Data are listed in Table S2. Error bars represent the 2σ uncertainties.

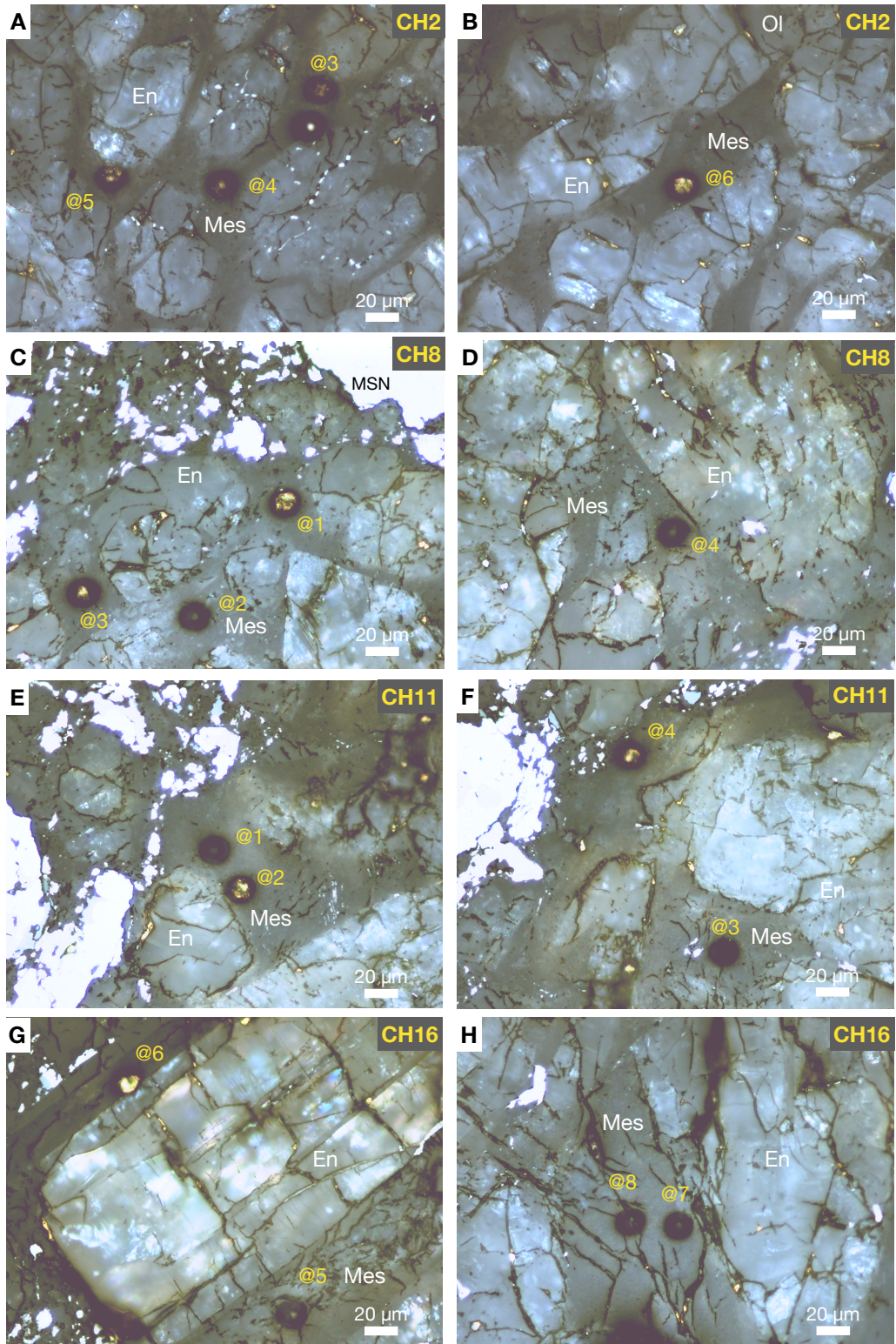


Fig. S6. Optical microscope images of SIMS spots after measurements in the mesostasis of Sahara 97096 chondrules. Spots of chondrule CH2 are shown in A and B panels, of chondrule CH8 in C and D panels, of chondrule CH11 in E & F panels, and of chondrule CH16 in G & H panels. Numbers refer to analyses shown in Table S4. Mes = Mesostasis, En = enstatite clinopyroxene, Ol = olivine, MSN = metal sulfide nodule (outside chondrule).

Table S1. Average and standard deviation (SD) of bulk-rock hydrogen abundances and isotopic ratios standard analyses. SO 188, Musc D65 and Mica Mg were used for the correction of instrumental mass fractionation on H isotopic composition. SD = standard deviation. N = number of measurements. Relat. = 2SD / average in percent.

Standard	N	H (wt. %)			H ₂ O (wt.%)		δD_{SMOW} (‰)	
		Average	2SD	Relat.	Average	2SD	Average	2SD
SO 188	34	0.489	0.025	5.1%	4.40	0.22	-83.6	3.4
Musc D65	33	0.479	0.045	9.3%	4.32	0.40	-86.7	2.8
Mica Mg	32	0.287	0.023	7.9%	2.58	0.20	-76.7	2.5
GMR-KS12	4	0.037	0.006	15.6%	0.33	0.05	-82.2	6.4
SR2-02	6	0.025	0.005	21.8%	0.23	0.05	-85.6	3.8
GSJ-JB3	5	0.018	0.005	27.0%	0.16	0.04	-116.4	7.6
CYP78	6	0.011	0.004	39.6%	0.10	0.04	-103.3	12.6

Table S2. Bulk-rock hydrogen contents and isotopic compositions of enstatite chondrites and different lithologies of the Norton County aubrite. Classification (Classif.) and petrologic type of the samples are also reported. Hydrogen isotopic compositions are reported normalized to standard mean ocean water (SMOW, $D/H_{SMOW} = 0.00015576$). The 2σ uncertainties (Uncert.) on hydrogen (H or H_2O equivalent) concentrations correspond to the reproducibility extrapolated from reference materials (see text). Reproducibility of δD_{SMOW} is estimated to be $\leq 5\%$ from replicate analyses of samples and reference materials (see text). Sahara 97116 and Sahara 97096 are two fragments of the same meteorite. The bulk rock results for the EH3 Kota-Kota and Caleta El Cobre 025 chondrites are reported here but not considered in the Fig. 1 and the discussion due to possible terrestrial contamination (see text). Equiv. H_2O = hydrogen content reported in water equivalent.

Meteorite	Classif.	H (wt.%)	Uncert. (2σ)	equiv. H_2O (wt.%)	Uncert (2σ)	δD_{SMOW} (‰)	
Sahara 97116	EH3	0.060	0.010	0.54	0.08	-103.0	
		0.056	0.010	0.51	0.08	-104.1	
		0.050	0.009	0.45	0.08	-103.0	
		0.045	0.008	0.40	0.07	-104.3	
Yamato-791790 [§]	EH3	0.037	0.008	0.33	0.06	-107.8	
Indarch*	EH4	0.037	0.008	0.34	0.06	-97.8	
Abee*	EH4	0.022	0.006	0.20	0.05	-105.9	
		0.021	0.006	0.19	0.05	-105.7	
Saint Sauveur*	EH5	0.038	0.008	0.34	0.06	-125.0	
Saint Mark's*	EH5	0.025	0.006	0.23	0.05	-115.8	
		0.022	0.006	0.20	0.05	-107.5	
Eagle*	EL6	0.046	0.009	0.41	0.07	-119.5	
		0.022	0.006	0.20	0.05	-115.1	
Daniel's Kuil*	EL6	0.021	0.005	0.19	0.05	-132.5	
		0.016	0.005	0.15	0.04	-131.4	
Hvittis*	EL6	0.010	0.004	0.09	0.03	-129.5	
		0.009	0.003	0.08	0.03	-137.2	
Khairpur*	EL6	0.015	0.005	0.13	0.04	-126.6	
		0.013	0.004	0.12	0.04	-125.3	
Pillistfer*	EL6	0.015	0.005	0.14	0.04	-144.3	
		0.014	0.004	0.13	0.04	-146.5	
Norton County* grey	Aubrite	0.022	0.006	0.20	0.05	-111.4	
		dark	0.013	0.004	0.12	0.04	-113.8
		enstatite	0.059	0.010	0.53	0.08	-154.8
Kota-Kota	EH3/alt.	0.117	0.015	1.05	0.12	-108.8	
		0.105	0.014	0.95	0.12	-106.0	
Caleta El Cobre 025	EH3/alt.	0.102	0.014	0.92	0.11	-127.6	
Sahara 97116 alt. border	EH3/alt.	0.303	0.025	2.73	0.21	-132.3	

	.	0.226	0.021	2.00	0.18	-136.6
Sahara 97096 rusty crust	EH3/alt.	0.471	0.033	4.24	0.27	-140.1
Orgueil*	CI	0.838	0.045	7.5	0.4	+143.2
		0.909	0.047	8.2	0.4	+146.0
		1.009	0.050	9.1	0.5	+131.0
		0.965	0.049	8.7	0.4	+131.9
Alais*	CI	0.931	0.048	8.4	0.4	+143.9
		0.996	0.050	9.0	0.4	+123.4
Murchison*	CM2	0.865	0.046	7.7	0.4	-75.2
		0.799	0.044	7.2	0.4	-74.6

*Observed falls. § Antarctic find, presence of terrestrial weathering.

Table S3. Elemental and isotopic compositions of the standard glasses measured using SIMS for the calibration of the instrumental mass fractionation. N = number of SIMS analyses; SD = standard deviation; SE = standard error of the mean; α = instrumental fractionation factor with $\alpha = (D^+/H^+)/(D/H_{\text{ref}})$.

Type	Name	Ref.	H ₂ O (wt%)	SiO ₂ (wt%)	H ₂ O/SiO ₂	D/H _{ref} (x10 ⁻⁶)	N	¹ H ⁺ / ³⁰ Si ⁺	2SD	2SE	D ⁺ /H ⁺ (x10 ⁻⁶)	2SD (x10 ⁻⁶)	2SE (x10 ⁻⁶)	α
Basalt	Etna-0	this study	1.350	46.8	0.0288	133	35	0.397	0.044	0.007	95.6	3.81	0.64	0.72
Basalt	60701	(59)	0.630	49.1	0.0128	146	18	0.166	0.017	0.004	109	3.70	0.87	0.75
Basalt	47963	(59)	1.450	48.2	0.0301	144	14	0.389	0.029	0.008	108	4.39	1.17	0.75
Basalt	40428	(59)	0.850	50.4	0.0169	144	9	0.229	0.011	0.004	104	9.70	3.23	0.72
Andesite	Tan25-0	this study	0.850	60.2	0.0141	126	23	0.202	0.038	0.008	88.9	5.68	1.18	0.70
Andesite	T1-G	(60)	0.026	58.5	0.0004	138	8	0.003	0.000	0.000	104	24.6	8.68	0.76
Dacite	StHs6/80	(60)	0.025	63.7	0.0004	141	19	0.005	0.000	0.000	109	24.6	5.63	0.77
Rhyolite	MC84-df	(61)	0.700	76.4	0.0092	145	25	0.397	0.044	0.007	103	8.63	1.73	0.71
Phonolite	L-10	(44)	0.01	54.34	0.0002	n.m.	3	0.166	0.017	0.004				
Phonolite	L-1	(44)	1	54.34	0.0184	n.m.	3	0.389	0.029	0.008				
Phonolite	L-9	(44)	1.63	54.34	0.0300	n.m.	3	0.229	0.011	0.004				

Table S4. Water contents and H isotopic ratios measured using SIMS in chondrule mesostases of the enstatite chondrite Sahara 97096 (EH3), and the CV-type carbonaceous chondrites Vigarano and Kaba for comparison. Classif. = Classification; SE = standard error of the mean.

Meteorite	Classif.	Chondrule	Analysis number	H ₂ O (wt. ppm)	2SE	δD (‰)	2SE		
Sahara 97096	EH3	CH2	@3	9819	48	-185	21		
		CH2	@4	8894	54	-152	22		
		CH2	@5	11081	92	-165	22		
		CH2	@6	5104	15	-145	25		
		CH16	@5	2701	142	-146	24		
		CH16	@6	7823	43	-95	23		
		CH16	@7	2865	139	-205	26		
		CH16	@8	2965	78	-146	28		
		CH11	@1	8416	91	-121	24		
		CH11	@2	6726	35	-124	23		
		CH11	@3	4367	78	-123	27		
		CH11	@4	9040	83	-111	28		
		CH8	@1	10898	83	-171	22		
		CH8	@2	8872	141	-151	23		
		CH8	@3	12277	69	-201	21		
		CH8	@4	9089	452	-116	23		
				n = 16	Average	7559	Average	-147	
			2SD	6184	2SD	64			
			2SE	1546	2SE	16			
Vigarano	Cvred	Ch-4	@1	301	7	-263	21		
		Ch-4	@2	235	10	-233	24		
		Ch-4	@3	127	3	-245	22		
		Ch-4	@4	700	19	-222	24		
		Ch-11	@1	347	10	-297	19		
		Ch-11	@2	208	12	-233	24		
		Ch-11	@3	193	14	-325	23		
		Ch-11	@4	546	17	-267	22		
				n = 9	Average	332	Average	-261	
			2SD	392	2SD	71			
			2SE	139	2SE	25			
Kaba	CVoxB	CH3	@1	133	4	-143	30		
		CH3	@4	267	9	148	38		
		CH6	@2	476	10	-26	29		
		CH6	@4	192	8	-2	46		
		CH7	@1	123	3	-33	40		
		CH7	@2	62	2	157	53		
				n = 10	Average	209	Average	17	
					2SD	296	2SD	232	
			2SE	121	2SE	95			

Table S5. Data of CI-type carbonaceous chondrites and ECs taken for the calculation of the mixing proportions necessary to reproduce the Earth surface H and N isotopic compositions. EC values correspond to the averaged value of the least metamorphosed chondrites (EH3) measured in the present study.

	CI	Ref.	EC	Ref.	Surface
D/H	174.0×10^{-6}	(7)	139.5×10^{-6}	this study	155.76×10^{-6}
δD	+117‰	(7)	-104‰	this study	0
[H]	10.3 wt.%	(7)	0.45 wt.%	this study	–
$^{15}\text{N}/^{14}\text{N}$	3.691×10^{-3}	(7)	3.667×10^{-3}	(34)	3.677×10^{-3}
$\delta^{15}\text{N}$	+39‰	(7)	-28‰	(34)	0
[N]	0.2 wt.%	(7)	0.05 wt.%	(34)	–

Table S6. Water contents and H isotopic ratios reported in literature, showing the paucity of and large discrepancies within the existing data for enstatite meteorites. n.m. = not measured

Meteorite	Type	H ₂ O (wt.%)	δD (‰)	Reference
Abee* (Magnetic)	EH4	0.15	-135	(62) [±]
Abee* (Non-magnetic)	EH4	0.06	-163	(62) [±]
Abee*	EH4	0.20	-67.8	(9) [§]
ALHA77295	EH4	0.82	n.m.	(63)
Hvittis*	EL6	0.11	-78.1	(9) [§]
Eagle*	EL6	0.43	n.m.	(63)
Happy Canyon	EL6	4.60	n.m.	(63)
Pillistfer*	EL6	<0.1	n.m.	(63)

*observed falls; §reported in (9) as unpublished data; ±from stepwise heating, in which two fractions of the bulk chondrite were measured separately

Caption for Data S1 (separate file)

Excel spreadsheet tabulating the bulk rock hydrogen contents and isotopic compositions measured by EA-IRMS (includes data of Table S2 and the amount of sample measured in each analysis in milligram) & the SIMS hydrogen content, hydrogen isotopic composition and chemical compositions of the chondrule mesostases (includes data from Tables S2 & S4).